The Binding and Regioselectivity of Reaction of (R)- and (S)-Nicotine with Cytochrome P-450cam: Parallel Experimental and Theoretical Studies

Jeffrey P. Jones,*,‡ William F. Trager,† and Timothy J. Carlson†

Contribution from the Department of Pharmacology, University of Rochester, Rochester, New York 14642, and the Department of Medicinal Chemistry, University of Washington, Seattle, Washington 98195. *Received June 18, 1992*

Abstract: (S)- and (R)-nicotine were used to test a theoretical model for the binding and regioselectivity of cytochrome P-450. Theoretical studies predict that the binding of (R)-nicotine will be more favorable than the binding of (S)-nicotine by between 0.400 and 0.600 kcal. A parallel experimental study determined that the binding constants differed by 0.333 kcal. The overall metabolic rate of (R)-nicotine is 1.4-fold faster than (S)-nicotine which is consistent with the predicted difference in binding energy. Product formation is theoretically predicted to occur at a faster rate at the 5′ methylene group than at the N-methyl group of the pyrrolidine ring for both enantiomers. This prediction was confirmed by the experimental results. The factors that are important in the differential binding of the two enantiomers are discussed. The agreement between theory and experiment indicates that the force field used in these calculations may be of general applicability for the prediction of the binding of substrates to P-450cam.

The cytochrome P-450 (CYP) family of enzymes is critical in the homeostasis of all mammalian species and is present in plants and bacteria. CYP enzymes are important in steroid, eicosanoid, and retinoid metabolism as well as in the metabolism of xenobiotics. Numerous pesticides and environmental pollutants are oxidized by the CYP enzymes to reactive intermediates and products that are potentially toxic and/or carcinogenic. For example, epoxides, N-hydroxyl amines, benzyl alcohols, alkenes, and acid halides are all formed by CYP-catalyzed reactions and are directly or indirectly related to the adverse effects associated with their parent compounds. In fact, Guengerich and Shimada[1] have proposed that the majority of oxidative bioactivation reactions are attributable to CYP. The pivotal role of CYP in chemical carcinogenesis and toxicity suggests that CYP is an ideal system from which to begin to develop correlations between theory and experiment for predicting bioactivation to potentially toxic intermediates. The CYP enzyme family has the following additional properties that make it an excellent target for theoretical experiments; (1) it has broad substrate selectivity (i.e., the enzymes will oxidize almost any organic molecule that can reach the catalytic site), (2) a high-resolution crystal structure for one of the isoforms is available to use as a model for the family, and (3) the primary role of this enzyme system is to activate molecular oxygen rather than to stabilize the transition state for the conversion of substrate to product. This is important since specific stabilization of the transition state, by the apoprotein, is difficult to model theoretically.

In an attempt to understand the mechanism of CYP, several small-molecule quantum chemical studies have been performed.[2-6] Most of these studies have concentrated on the chemical mechanism of the various reactions catalyzed by the CYP superfamily. Of these studies, only the method of Korzekwa et al.[6] attempts to predict the relative reactivity of different substrates. The method of Korzekwa et al. has been successful in predicting the LD_{50} of nitrile containing compounds in mice[7] and in predicting the in vivo rate of metabolism of hydrochlorofluorocarbons.[8]

The binding characteristics of a few substrates were addressed using molecular mechanics.[9,10] These studies had qualitative success in predicting the regioselectivity for the reaction of valproic acid and styrene, but do not address the relative reactivity of different compounds. This approach, as it has been implemented, can only predict the relative rates of two reactions that occur from the same substrate and not the relative rates of a similar reaction with two different substrates. Finally, in the most thorough study to date, the binding characteristics of camphor and norcamphor were described by Ornstein and co-workers.[11]

Until recently, it was believed that CYP101 (cytochrome P-450cam) would only accept substrates related to camphor. However, a recent study has established that substrates from mammalian CYP enzymes are also substrates for CYP101.[9] In this paper we report that the two enantiomers of nicotine are substrates for CYP101 and compare the experimental metabolism of these compounds with the results of theoretical predictions. Free energy perturbation and molecular dynamics calculations on the binding of (S)- and (R)-nicotine to CYP101 give very close agreement with experimental results. Qualitative agreement is also seen between the predicted and experimental values for regioselectivity. These theoretical results allow for the determination of the steric and electrostatic factors that are important in CYP mediated oxidations. These results, combined with the quantum chemical method of Korzekwa et al.,[6] allow for the theoretical evaluation of a number of the factors that are involved in determining the reactivity of this important family of enzymes.

Experimental Section

Synthesis of Deuterated Nicotines. The general procedure of Jacob,[12] with the following modifications was used to generate racemic nornicotine-2′-d_1. Sodium hydride (5 g of a 60% dispersion in mineral oil, 125 mmol) contained in a 500-mL flask was washed free of mineral oil with toluene. The flask was charged with 150 mL of THF. A solution of ethyl nicotinate (13 g, 86 mmol) and N-vinylpyrrolidine (11 g, 100 mmol) in 25 mL of THF was then added in one portion. The mixture

† University of Washington.
‡ University of Rochester.

(1) Guengerich, F. P.; Shimada, T. *Chem. Res. Tox.* **1991**, *4*, 391-407.
(2) Shea, J. P.; Nelson, S. D.; Ford, G. P. *J. Am. Chem. Soc.* **1983**, *105*, 5451-5454.
(3) Loew, G. H.; Goldblum, A. *Mol. Pharm.* **1985**, *27*, 375-386.
(4) Koymans, L.; van Lenthe, J. H.; van de Straat, R.; Donne'-Opden Kelder, G. M.; Vermeulen, N. P. E. *Chem. Res. Tox.* **1989**, *2*, 60-66.
(5) Korzekwa, K. R.; Trager, W. F.; Gouterman, M.; Spangler, D.; Loew, G. H. *J. Am. Chem. Soc.* **1985**, *107*, 4273-4279.
(6) Korzekwa, K. R.; Jones, J. P.; Gillette, J. R. *J. Am. Chem. Soc.* **1990**, *112*, 7042-7046.
(7) Grogan, J.; Pearlman, R. S.; DeVito, S. C.; Korzekwa, K. R. *Chem. Res. Tox.* **1992**, *5*, 548-552.
(8) Harris, J. W.; Jones, J. P.; Martin, J. L.; LaRosa, A. C.; Olson, M. J.; Pohl, L. R.; Anders, M. W. *Chem. Res. Tox.* **1992**, *5*, 720-725.
(9) Ortiz de Montellano, P. R.; Fruetel, J. A.; Collins, J. R.; Camper, D. L.; Loew, G. H. *J. Am. Chem. Soc.* **1991**, *113*, 3195-3196.
(10) Collins, J. R.; Camper, D. L.; Loew, G. H. *J. Am. Chem. Soc.* **1991**, *113*, 2736-2743.
(11) (a) Bass, M. B.; Paulsen, M. D.; Ornstein, R. L. *Proteins: Struc. Func. Genet.* **1992**, *13*, 26-37. (b) Paulsen, M. D.; Ornstein, R. L. *Proteins: Struc. Func. Genet.* **1991**, *11*, 184-204.
(12) Jacob, P., III *J. Org. Chem.* **1982**, *47*, 4165-4167.

0002-7863/93/1515-381$04.00/0

was refluxed for 1 h and then cooled to room temperature. Concentrated HCl (15 mL) diluted with H_2O (25 mL) was added and the THF was evaporated. Additional HCl (25 mL) and H_2O (50 mL) was added, and the mixture was refluxed overnight. The mixture was made basic with NaOH and extracted with methylene chloride (3 × 75 mL). The pooled extracts were washed with H_2O and the solvent was evaporated. A bulb-to-bulb vacuum distillation resulted in a pale yellow liquid which solidified in the receiver (9.0 g, 62%). The structural characteristics were consistent with myosmine.[13]

Myosmine (1.5 g, 10.2 mmol) was dissolved in 18.5 mL of methanol-d_1 and 4.5 mL of acetone. Sodium borodeuteride (1.2 g, 28.7 mmol) was added slowly while the reaction stirred at 0 °C. A drying tube was connected, and the reaction was allowed to stir for 4 h at room temperature. The mixture was made basic and extracted with methylene chloride. Evaporation of solvent yielded a yellow oil which by TLC was a mixture of myosmine and nornicotine. The compounds were separated by silica gel flash chromatography (85:15:0.25) proportions of $CH_2Cl_2/CH_3OH/N(CH_2CH_3)_3$) to yield 0.92 g of nornicotine-2′-d_1 (61%).

A method involving the preparative scale HPLC separation of nornicotine derivatives was used[14] to resolve the racemic, monodeuterated nornicotine. 1*R*,2*S*,5*R*-methylchloroformate (0.968 mL, 4.51 mmol) was added dropwise to a solution of 0.65 g of nornicotine-2′-d_1 (4.36 mmol) and 0.93 mL of triethylamine in 25 mL of ether. The mixture was stirred at 0 °C for 15 min under argon and then at room temperature for 1.5 h. The mixture was filtered, and the yellow filtrate was washed with 25 mL of 10% aqueous NaOH. The ether solution was dried with $MgSO_4$ and evaporated to yield a dark yellow oil. Silica gel flask chromatography (solvent system: 9:1.5 CH_2Cl_2/CH_3OH) was carried out to purify the methylchloroformate derivative.

In our hands separation of the resulting diastereomers was not achieved using the normal phase HPLC method of Seeman.[14] We were able to achieve good separation, however, using a Beckman Ultrasphere C18 column (5 μM pore size, 250 mm length, and 10 mm i.d.). The mobile phase was 65:35 CH_3CN/acetate buffer (10 mM, pH 4). A stock solution of 100 mg of the diastereomeric mixture per mL of mobile phase was prepared and repeated injections of 0.08 mL were made. A flow rate of 4.0 mL/min was used, and the resulting retention times of the two diastereomers were approximately 15 and 17 min. The separate fractions were reduced in vacuum and the remaining aqueous solvent was extracted with methylene chloride. The diastereomeric purity of the fractions was determined by gas chromatographic analysis with a DB-5 capillary column at 250 °C. Samples corresponding to urethane derivatives of >98.5% diastereomeric purity were subsequently hydrolyzed under acid conditions as described[13] to yield resolved, monodeuterated nornicotine (typical yield of hydrolysis was 89.5%).

Methylation of the resolved nornicotine was carried out using formic acid and formaldehyde.[15] Resolved nornicotine-d_1 (38.1 mg, 0.257 mmol) was placed in a Reacti-Vial, to which was added 177.6 mL of 9.6% formic acid (0.369 mmol) followed by 384.6 mL of 3.2% formaldehyde (0.38 mmol). The reaction was stirred at 80 °C for 20 h. A basic extraction with 3 × 5 mL methylene chloride, followed by drying (K_2CO_3) and evaporation, yielded 33.4 mg of nicotine (80%). Proton NMR and GC analysis indicated pure nicotine [300-MHz ^{1}H NMR ($CDCl_3$) d 1.65–1.9 (m, 2, C3′ and C4′), 1.9–2.05 (m, 1, C4′), 2.15 (s, 3, NCH_3), 2.25 (m, 1, C3′), 2.3 (q, 1, C5′), 3.1 (t, 0.05, C2′), 3.25 (t, 1, C5′), 7.3 (m, 1, C5), 7.6 (d of t, 1, C4), 8.3–8.5 (m, 2, C2 and C6)]. The NMR spectrum confirmed the position of a deuterium atom at the C-2′ position by showing a marked decrease in the area of the triplet at 3.1 ppm. Selected ion monitoring analysis of the base peak of the mass spectrum (m/z 84, 85, 86) indicated 95.8% incorporation of one deuterium. HPLC with a chiralcel OD column was used to assess enantiomeric purity of the nicotine. The sample which corresponded to the first urethane derivative peak from the preparatory scale separation was found to be (*R*)-nicotine (98.2% R, 96.4 ee). Chromatographic conditions for the chiralcel column were a mobile phase of hexane/isopropyl alcohol/triethylamine (95:5:0.02) and a flow rate of 0.5 mL/min.

The pseudoracemate was prepared by making separate stock solutions of approximately equal concentrations of (*S*)-nicotine-d_0 and (*R*)-nicotine-2′-d_1 in methanol. The concentrations were assessed by monitoring the UV absorbance at 262 nm (the λ_{max} of nicotine) and then the appropriate volumes of the stock solutions were mixed to yield a 1:1 molar ratio of (*R*)- to (*S*)-nicotine. The solvent was evaporated, and the pseudoracemate was dissolved in acidic water (pH 3) to make a stock solution for use in the enzymatic reactions.

(13) Brandage, S.; Lindblom, L. *Acta Chem. Scand. B* **1976**, *30*, 93.
(14) Seeman, J. I.; Chavdarian, C. G.; Secor, H. V. *J. Org. Chem.* **1985**, *50*, 5419–5421.
(15) Pine, S. H.; Sanchez, B. L. *J. Org. Chem.* **1971**, *36*, 829–832.

N′-Dideuteromethylnornicotine (nicotine-d_2) was synthesized by the formic acid/formaldehyde reaction described above with a deuterated formaldehyde solution. The deuterated formaldehyde solution was prepared by dissolving deuterated paraformaldehyde in D_2O. The yellow oil obtained from the reaction was purified by silica gel chromatography (88:12 CH_2Cl_2/CH_3OH) and analyzed by proton NMR and mass spectrometry. Proton NMR (300 MHz) indicated the position of the deuteriums by the marked decrease in the methyl proton peak of nicotine at 2.15 ppm. Selected ion monitoring of the base peak of the mass spectrum (m/z 84, 85, 86) indicated 98.1% incorporation of two deuteriums in the product.

Enzyme Isolation. We modified the method of Wagner and Gunsalus[16] to obtain purified CYP101 as follows. *Pseudomonas putida* was transferred to 20 mL of L-broth[17] and incubated at 30 °C for 10 h. The broth, 10 mL, was transferred to 400 mL of a phosphate–ammonia solution containing 10 mM glutamate as a carbon source. After 2 h camphor, 2 mmol from a 3 M stock solution in DMF, was added. When the OD_{660} reached 2, 50 mL of this solution was transferred into 400 mL of the phosphate–ammonia solution with camphor (2 mmol initially and another 2 mmol after the OD reached 1) as the sole carbon source and the mixture incubated for 8 h or until the OD_{660} reached 2. All 450 mL was then transferred to four separate flasks with a total volume of 2.5 L. Camphor was added in 6 mmol aliquots every hour. The OD_{660} was monitored and when the absorbance reached ca. 5 the cultures were centrifuged at 10000 g for 40 min. The pellets were frozen at −78 °C. To lyse the cells the pellet was allowed to thaw slowly at room temperature. Potassium phosphate buffer with DNAse, RNAse, and lysozyme (ca. 3 mg of each) was added to the thawed cells, and the mixture was refrigerated for 12 h. The mixture was centrifuged at 100000 g for 65 min and the supernatant frozen. At this stage approximately 500 nmol of CYP was present as determined by carbon monoxide difference spectra. This fraction could be used for most metabolic studies after the removal of camphor by passing the solution over a Sephadex G-15 size exclusion column. The enzyme was used immediately after removal of the camphor.

Determination of Spectral Dissociation Constants. The spectral dissociation constant was measured by placing CYP101 in 50 mM pH 7.4 Tris buffer at 30 °C in 1 mL total volume. Various concentrations of either (*R*)- or (*S*)-nicotine were added as the hydrochloride salt in water (extinction coefficient at 262 nm is 2951 A $(M)^{-1}$ $(cm)^{-1}$) and difference spectra recorded. The spectral dissociation constant was calculated by the difference in absorption between the peak (431) and the trough (414 nm) versus concentration. A nonlinear least-squares fit of the resulting data to a hyperbola was used to determine the maximum change in absorption and the K_s. The K_s value was determined to be 59.8 ± 5.5 μM (N = 10) for (*S*)-nicotine and 34.4 ± 3.9 μM (N = 9) for (*R*)-nicotine.

Metabolism and Regioselectivity. Incubations with the pseudoracemate included 1 nmol of CYP101, 1 mM substrate, 1 mM NaCN, and 1 mM NADH in 50 mM potassium phosphate buffer, pH 7.0, all in a final volume of 1 mL. Addition of NADH initiated the incubation. After 20 min, the incubation was terminated by addition of 0.5 mL of acetone. The pH of the incubation mixtures was adjusted to 10, and extracted with 3 × 2 mL of pentane. The solvent was evaporated, and the residue was taken up in 25 μL of ethyl acetate. The samples were analyzed by GC/MS analysis of the cyanide adducts of the iminium ion products of nicotine oxidation.[18] The base peaks of the two cyano adducts (m/z 109 for protio products and m/z 110 for the monodeuterated products) were analyzed in the selected ion monitoring mode.

Incubations examined for the depletion of substrate contained 2 nmol of P450cam, either 50 or 25 μM nicotine, and 1 mM NADH in 50 mM KP buffer, pH 7.0. Additionally, incubations were done in the presence and absence of 1 mM NaCN. No effect on the rate of nicotine oxidation was observed. Termination of the enzyme reaction was accomplished by addition of 0.5 mL of acetone, followed by addition of 50 nmol of internal standard *N*′-dideuteromethylnornicotine in 100 mL of ethanol. The incubations were then extracted as above. Nicotine concentrations were determined by GC/MS analysis of the ratio of nicotine-d_0 to internal standard. A standard curve of peak area ratios versus concentration ratios for nicotine-d_0 and nicotine-d_2 was developed and used in the quantitation.

Parameter Development. In an attempt to determine accurate point charges for the molecular dynamics calculations quantum chemical studies were performed on the heme complex of CYP101. The coordinates of the heme–iron–sulfur complex were taken from the crystal structure of CYP101 with substrate bound (structure 2cpp from the Brookhaven data bank). The full porphyrin was used including all side chains, and the porphyrin propionate groups were not protonated. Thiomethane anion was substituted for the cysteine residue and the methyl group placed in the same orientation as the methylene group of

Table I. Charge Assigned the Porphyrin of CYP101 by ab Initio Calculation Using the LANL1MB Basis Set[a] without Oxygen Bound and with Oxygen Bound

atom	Mulliken charge	NBO charge	NBO charge with O
Fe	0.813	1.39	1.29
S	−0.710	−0.911	−0.888
N	−0.288	−0.383	−0.316
O_{Fe}	na	na	−0.054

[a] Complete charges are given in the supplementary material along with the AMBER prep files.

the cysteine. The charges were determined using the Gaussian 90 ab initio package, the LANL1MB basis set. This basis set has relativistic corrections for outer core electrons.[19] Natural populations analysis was performed using the method of Reed and Weinhold.[20] The charges were determined for the sextet spin state using the UHF ab initio level of theory. Since this was an unrestricted Hartree–Fock calculation the spin was not constrained to a sextet (S^2 = 12.2). The spin state is thus not a true sextet but contains a large amount of spin contamination. This might be expected for such a large highly conjugated structure. The spin contamination in effect includes to some extent the electron correlation which is not included in a spin restricted calculation. Since the spin restricted calculation is more expensive and it is not known whether it would give better point charges, we choose to use the UHF values. It should be noted that since the point charge model is not a very realistic approximation of the charge distribution, in effect the calculations only act as a guide for guessing the appropriate charges that will hopefully reproduce experimental values. The ultimate utility of the point charges depends on the ability of the values to reproduce experiment. The charges for selected atoms are reported in Table I. As expected the charges determined using natural population analysis[20] were significantly different from charges determined by Mulliken population analysis. Natural population analysis is expected to give much better charges for ionic and highly polar species than Mulliken population analysis.[21]

The minimum energy nicotine structure was found using the semiempirical MNDO Hamiltonian. The structure obtained by this method was in close agreement with the crystal structure of nicotine.[22] Although the crystal structure is of a hydrogen iodide salt the RMS deviation is only 0.29 Å. The charges for the nicotine were determined using the ESP program of Besler and Merz[23] in MOPAC version 6[24] and corrected to approximate the 6-31G* basis set charges. The force constants were taken from the standard AMBER values.[25] The AMBER minimized structure was essentially identical to the MOPAC minimized structure. Although no average structure was determined for a given dynamics run, a random sample of nicotine structures during several dynamics runs indicate that while inversion occurs at the pyrrolidine nitrogen and rotation occurs at the pyridine–pyrrolidine bond no substantial distortion of the bond lengths or ring angles is observed at 303 K.

Systematic errors, due to sampling errors or to force field associated errors, may influence the free energy calculations for the enzyme–substrate complex.[26] To determine if the perturbation of nicotine from one enantiomer to another could give an artifactual difference in free energy we performed a free energy calculation in which (*S*)-nicotine was converted to (*R*)-nicotine in a solvent box. The (*S*)-nicotine was placed in a 19 × 19 × 19 Å box of TIP3P water. First, the solvent around the box was minimized. Second the solute was minimized. Finally, the whole system was minimized. The system was equilibrated for 10 ps at a constant temperature of 303 K and constant pressure using periodic boundary conditions. For the nonbonded interactions of 8 Å cutoff distance was employed and nonbonded interaction list was updated every 50 steps. Since the two enantiomers must have the same solvation energy

Table II. Gibbs Free Energy of (*R*)-Nicotine Minus That of (*S*)-Nicotine in a Water Solvent Box

method	simulation direction	simulation time (ps)	$\Delta\Delta G$[a]
slow growth	$R \rightarrow S$	99	0.239 ± 0.222[b]
slow growth	$S \rightarrow R$	99	−0.145 ± 0.222
slow growth	$R \rightarrow S$	200	0.061 ± 0.043
slow growth	$S \rightarrow R$	200	0.135 ± 0.043
dynamic windows	$S \rightarrow R$	60	−0.025 ± 0.035[c]
dynamic windows	$R \rightarrow S$	60	−0.074 ± 0.035

[a] Free energy difference in kcal. [b] The error is the standard deviation of the runs in forward and reverse direction for each simulation time. For the slow growth simulations this is the average of four numbers, two for each simulation are obtained by double wide sampling. [c] No double wide sampling was performed on the dynamic windowing values.

Table III. Free Energy Difference, $\Delta G(S) - \Delta G(R)$, for the Binding of (*S*)-Nicotine and (*R*)-Nicotine to CYP101

method	total time (ps)	energy difference[a]
experimental[b]		0.333
windows	80	0.621[c]
slow growth	99	0.488 ± 0.043[d]
slow growth	99	0.413 ± 0.043
dynamic windowing	≫100	0.510 ± 0.075[e]

[a] The free energy difference in kcal. [b] The experimental difference in energy determined from the spectral dissociation constants. [c] No double wide sampling performed. [d] The error for the slow growth calculations are reported as in Table II footnote *b*. [e] The error for this simulation is 0.5 times the difference in the absolute value of the simulation in the forward and reverse direction determined by double wide sampling.

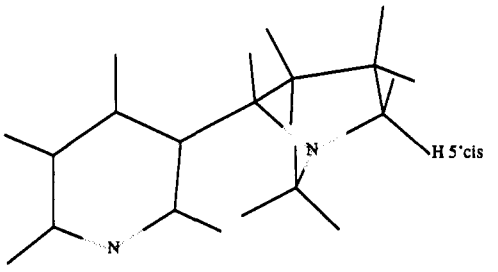

Figure 1. (*S*)-Nicotine.

in an achiral environment, this provides a good test for errors associated with the nicotine force field. Numerous calculations were performed using both the slow growth or dynamically modified windows. The average change in free energy for conversion of *R* to *S* is given in Table II. The results indicate that while for any given simulation the free energy change is not zero, the mean value of all the simulations is close to zero. These data indicate that no artefactual change in free energy is associated with the nicotine perturbation in an achiral environment. While this is not a perfect test of the validity of the protein–substrate model, it provides a rigorous test of the nicotine perturbation portion of the model.

The CYP101 crystal structure was obtained from the Brookhaven data bank. The energy of the entire enzyme complex was minimized using AMBER 3a. The all-atom model was used in each calculation with explicit inclusion of hydrogen atoms. These structures have been minimized with and without substrates bound, including in all cases the waters of crystallization but no external solvent. The crystal structure histidines were protonated by inspection of potential hydrogen bonding donors. Of the 13 histidines all but three external and one internal (H 80) had hydrogen bonds that could be easily assigned. A RMS deviation from the crystal structure of 0.59 Å was observed upon minimization. The force field for the heme portion, without oxygen bound to the enzyme, used charges from the ab initio calculations described above and the force constants determined by Lopez and Kollmann.[27] Each enzyme–substrate complex was minimized to a root-mean-squared gradient of less than 0.1 kcal/Å. We analyzed the dynamics runs from the AMBER calculations using Tripos Associates SYBYL program. Statistical analysis and dis-

(16) Gunsalus, I. C.; Wagner, I. C. *Methods Enzymol.* **1978**, *52*, 166–188.
(17) Lennox, E. S. *Virology* **1955**, *1*, 190–206.
(18) Peterson, L. A.; Trevor, A.; Castagnoli, N., Jr. *J. Med. Chem.* **1987**, *30*, 249–254.
(19) Hay, P. J.; Wadt, W. R. *J. Chem. Phys.* **1985**, *82*, 270–283.
(20) Reed, A. E.; Weinhold, F. *QCPE Bull.* **1985**, *5*, 141, Version 3.0.
(21) Reed, A. E.; Weinstock, R. B.; Weinhold, F. *J. Chem. Phys.* **1985**, *83*, 735–746.
(22) Barlow, R. B.; Howard, J. A. K.; Johnson, O. *Acta Crystallogr.* **1986**, *42*, 853.
(23) Besler, B. H.; Merz, K. M.; Kollman, P. A. *J. Comput. Chem.* **1990**, *11*, 431–439.
(24) Stewart, J. J. P., MOPAC Version 6, QCPE-455.
(25) Pearlman, D. A.; Case, D. A.; Caldwell, J. C.; Seibel, G. L.; Singh, U. C.; Wiener, P.; Kollman, P. A. AMBER 4; University of California, San Francisco, 1991.
(26) Beveridge, D. L.; Dicapua, F. M. *Annu. Rev. Biophys. Biophys. Chem.* **1989**, *18*, 431–492.
(27) Lopez, M. A.; Kollman, P. A. *J. Am. Chem. Soc.* **1989**, *111*, 6212–6222.

Table IV. Regioselectivity of CYP101 for (*R*)- and (*S*)-Nicotine[a]

substrate	methyl[b]	trans-5′ + cis-5′
(*S*)-nicotine	0.08	9.67
(*R*)-nicotine	0.72	12.57

[a] These results were quantified with the use of isotopically labeled products as internal standards. [b] μmol of product per incubation.

tance measurements were determined using the inhouse program DINKC. The temperature for all dynamics calculations was 303 K unless otherwise noted.

Results

Experimentally Determined Binding and Regioselectivity Differences between (*R*)- and (*S*)-Nicotine. The spectral binding constants were determined for each enantiomer of nicotine. The ratio of the two binding constants (*S*/*R*) was found to be 1.7. This ratio corresponds to a difference in binding affinity of 333 cal.

The results of the P450cam catalyzed oxidation of the pseudoracemic nicotine indicate that (*R*)-nicotine was preferentially oxidized over (*S*)-nicotine at all positions of oxidation. The *R* to *S* ratio was 1.30 for oxidation of nicotine at the 5′ position and 9.00 for oxidation at the methyl group (see Figure 1 for nicotine numbering scheme). The regioselectivity of reaction at various positions of each enantiomer, when they were incubated as a pseudoracemic mixture, was also determined. The amount of each cyano adduct that was formed in the incubations of the pseudoracemate is shown in Table IV. Both enantiomers favored oxidation at the 5′ position. The ratio of 5′-cyano adduct:methyl cyano adduct was 120 for (*S*)-nicotine and 17 for (*R*)-nicotine. These results are in general agreement with the theoretical prediction of regioselectivity (vide infra).

In order to approximate the relative total turnover for (*R*)-nicotine vs (*S*)-nicotine, we carried out substrate depletion studies. Substrate depletion was determined at an initial nicotine concentration of 50 μM. Values of v/s (which approximate V_{max}/K_m values when $s \ll K_m$) were calculated for both (*R*)- and (*S*)-nicotine. Typical values obtained were 0.0229/(min)(mL)(nmol CYP) for (*R*)-nicotine and 0.0164/(min)(mL)(nmol CYP) for (*S*)-nicotine. The *R*:*S* ratio of these values (a comparison of approximate V/K's) is 1.42, a value that correlates well with the spectral binding constants. Different preparations of CYP101 yielded slightly different catalytic activities, perhaps due to varying putidaredoxin reductase:CYP ratios. The greater depletion of (*R*)- versus (*S*)-nicotine, however, was consistent throughout the various enzyme preparations.

Theoretically Determined Binding and Regioselectivity Differences between (*R*)- and (*S*)-Nicotine. For our initial minimization (*R*)-nicotine was placed in the active site in approximately the same position as the bound camphor molecule in the crystal structure and the enzyme–nicotine complex was minimized. The system was heated to 303 K in three 100 K steps using short dynamics runs of 2 ps. The system was then equilibrated with 40 ps of dynamics at 303 K using a time step of 0.001 ps. The GIBBS program in AMBER was then used to determine the difference in energy of the two substrates bound in the CYP101 active site. Between each free energy run the resulting velocities were subjected to a 1–5 ps dynamics run to generate new starting velocities and trajectories. The initial configuration ($\lambda = 0$) was (*R*)-nicotine with a pentavalent pyridylic carbon. The fifth atom on the pyridyl carbon was a pro (*S*) dummy atom with a 0.3 Å bond length that grew during the calculation to a normal bond length of 1.08 Å. The *R* hydrogen atom was shrunk to 0.3 Å as the simulation progressed. No charge or steric energy was associated with the shrunken atoms in the initial and final states, respectively. This method has been reported to help to decrease errors associated with poor convergence of the system relative to a system in which the bond length remains constant and only the molecular radius is decreased.[28] Only specific amino acid residues that were in close proximity to the nicotine in the active site were allowed to move.

The best method for free energy perturbation analysis has not been determined. The three techniques used in this study include the slow growth method, the static windows method, and the dynamic windows method. The effect of simulation time was also explored. The simulations were performed in both directions, from $R \rightarrow S$ and from $S \rightarrow R$. Between each production run a short dynamics run was performed to give new trajectories. We found that all the techniques gave similar results and were in agreement with experiment. A description of the results follows and is summarized in Table III. When the windowing method was used, four windows were used with 10-ps equilibration prior to data collection for 10 ps in each window. The free energy change of the enzyme–substrate complex upon conversion of (*S*)- to (*R*)-nicotine was −0.621 kcal. The same starting velocities were used for a slow growth calculation. In this method (*R*)-nicotine was converted to (*S*)-nicotine over 10 ps. The free energy change using this method (ΔG, $S \rightarrow R$) was −0.58 kcal. Thus, both the windowing and slow growth method gave similar results. We increased the time for the slow growth calculation to 99 ps and used new starting trajectories from a 5-ps dynamics run. The result was a free energy change of 0.48 kcal upon mutation from (*R*)- to (*S*)-nicotine. When the same method was used in the reverse direction after another 5 ps of dynamics to generate another starting configuration the free energy change upon mutation from (*S*)- to (*R*)-nicotine was −0.41 kcal. One further experiment was performed using a new protocol, dynamically modified windows, in AMBER 4.0. The starting coordinates and trajectories were equilibrated further using 14 ps of dynamics. Each windows used 10 ps of equilibration followed by 10 ps of production. The windows were modified dynamically after the first two windows. The free energy change upon mutation of (*S*)- to (*R*)-nicotine was −0.586 kcal. The average of all of the simulations is 0.52 ± 0.08 kcal. Thus, the results of the simulations proved to be relatively independent of the time, method, and direction of the simulation. The average free energy change corresponds to the (*R*)-enantiomer binding with a 2.5-fold higher affinity than the (*S*)-enantiomer. All the values obtained compare favorably with the experimental difference in binding energy (see the spectral entry in Table III).

Table V. Mean Distances from the Iron–Oxygen Species of Each Hydrogen Atom at a Position of Reaction at 303 and at 1000 K

substrate	*N*-methyl	trans-5′	cis-5′
(*S*)-nicotine[a]	3.31	2.96	4.34
(*R*)-nicotine[a]	5.34	3.56	4.53
(*S*)-nicotine[b]	4.91	3.99	4.68
(*R*)-nicotine[b]	4.92	3.48	4.03

[a] From 100-fs snapshots of a 80-ps simulation at 303 K. [b] From 100-fs snapshots of a 40-ps simulation at 1000 K.

To predict the regioselectivity of reaction at various positions for each enantiomer, constant temperature dynamics were performed on CYP101 with oxygen bound to the iron. New charges were determined for the heme–oxygen complex using the ab initio basis and natural population analysis as described above for the Fe^{3+} heme without oxygen bound. Oxygen was added to the iron at a bond distance of 1.7 Å. A UHF calculation was then performed on the doublet spin state to determine the charges for the feryl–iron–oxygen species. The structure of the heme–iron–oxygen species is not known therefore the planar geometry of Edwards et al.[29] was used. The cysteine residue was modeled using a thiomethane anion. The iron–sulfur bond distance was 2.2 Å. The charges are given in Table I. Using these charges two separate 40-ps dynamics calculations were performed on each of the enantiomers. The distance between the hydrogen atoms of the nicotine and the active oxygen species were monitored by a series of 100-fs snapshots. The results are given in Tables V and VI.

Discussion

The stereoisomers of nicotine provide a subtle and specific tool to probe the active site of CYP101. Since both have the same solubility in water the free energy of solvation need not be considered in either the experimental or theoretical treatment of the binding of these compounds. Furthermore, the activation energy for the reaction of either enantiomer at the same relative position

Table VI. Number of Molecular Dynamics Pictures for Each Hydrogen Atom That Can Lead to Product within a Given Distance of the Oxygen in P450cam[a]

position of oxidation enantiomer/position	distance from the oxygen in Å				
	2.0	2.25	2.50	2.75	3.00
R/methyl	18	37	65	97	130
S/methyl	30	85	138	180	231
R/trans 5′	18	53	92	122	138
S/trans 5′	6	20	35	59	85
R/cis 5′	20	34	49	72	85
S/cis 5′	4	8	11	13	17

[a] Values are for 40-ps simulations at 1000 K.

should be the same unless unfavorable steric factors influence the catalytic complex or the transition state.[28] This leaves only the differences in the free energy of the bound enzyme–substrate complex to be evaluated.

The experimental determination of the binding of the two enantiomers gave values similar to those determined for pyridine. Pyridine binds with a K_D of 20 μM,[3] (*S*)-nicotine binds with a K_D of 59.8 μM, and (*R*)-nicotine binds with a K_D of 34.4 μM. The predicted difference (0.400–0.600 kcal) and experimental difference (0.333 kcal) in binding affinity between the two enantiomers are very close (see Table III). The small difference between the two is probably insignificant since the error in the theoretical calculation is only a mininum error and could be larger.[26] The main source of error in free energy perturbation calculations is from the short sample times that must be used for these calculations to be computationally feasible. The short sampling times mean that the whole rotational and translational surface will not be included in the calculation. This could make the placement of the substrate in the active site an important determinant of the outcome of the calculation. To overcome this problem we ran a dynamics run between each calculation to give new starting configurations. Two methods have been used to estimate the precision of the values obtained from free energy calculations. One, is to determine the difference of hysteresis for the same calculation performed in the forward and backward direction from the same starting geometry.[26] The average value for each entry plus or minus half the hysteresis of each run is very small or zero in all cases. Another method that will give larger error values is to compare the forward and backward values using different starting configurations;[32] this error is reported in Tables II and III. Each of the values in Table III were determined from a different starting configuration. It can be seen that the starting configuration has a profound effect on the outcome of the calculation. Since not all starting configuration can be tested the values obtained by this method will still only give a minimum error value. Furthermore, only one initial configuration of nicotine was docked and minimized to obtain the initial starting trajectories. Thus, the resulting values could be influenced by our initial model building method. If the nicotine model is docked incorrectly, it is possible that the agreement between theory and experiment is fortuitous.

The above discussion only considers the statistical error in free energy perturbation calculations. To determine if systematic errors associated with the perturbation of the nicotine molecule[27,28] led to a coincidental agreement with experiment we ran perturbation calculations on nicotine in a solvent box. Since (*S*)- and (*R*)-nicotine are enantiomers, the result should be no change in free energy. The results shown in Table II show that the mean value is close to 0. (The average for simulations of 40 ps or more is 0.012 kcal.) To our knowledge, this is the first time that this type

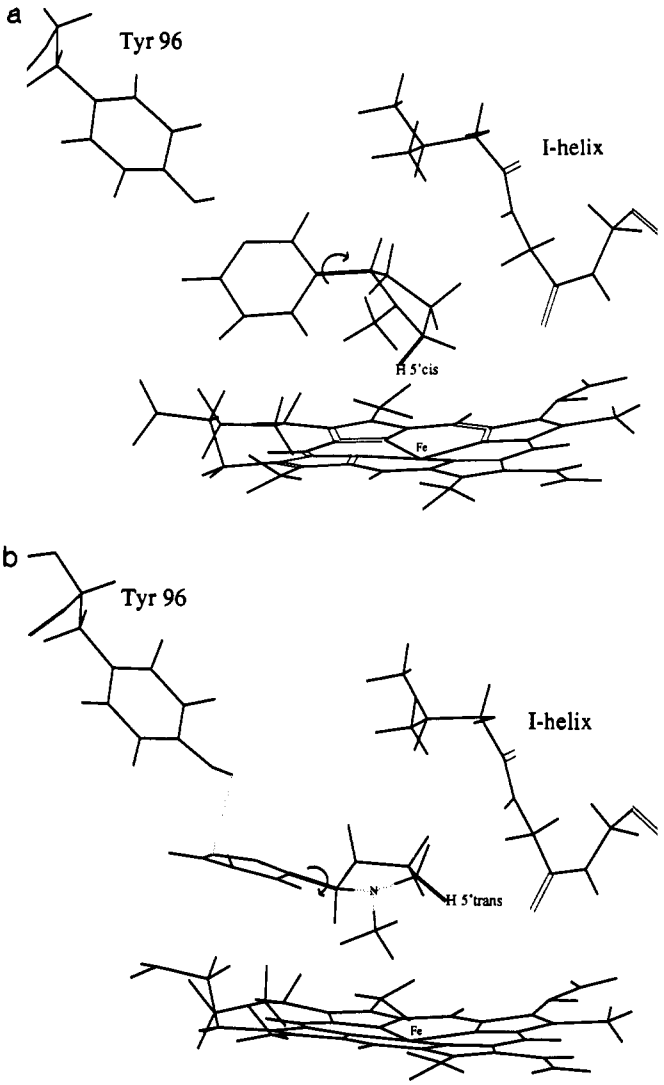

Figure 2. (a) The cis binding orientation of (*S*)-nicotine. Tyr96, Val247 Gly248, and Gly249 of the I-helix are shown. (b) The trans orientation of (*R*)-nicotine. The methyl groups of the pyrrole ring for both enantiomers are pointed up out of the plane. The nitrogen of the pyridine ring is not labeled, and the nitrogen in the pyrrolidine ring is not labeled for the (*S*)-enantiomer. The arrows indicate the bond where rotation occurs, and the light bond is the hydrogen bond between Tyr 96 hydroxyl group and the nitrogen of the pyridine ring.

of analysis has been used, and it may provide an insightful tool in determining the origins of errors in free energy perturbation calculations. We found that the water calculation gave much more hysteresis at shorter simulation times and much more overall error than the enzyme-substrate calculation. This is probably due to the increased translational freedom associated with the solvent compared to that of the enzyme. The enzyme can only undergo a limited number of rotational motions in order to relieve stereoelectronic repulsion, while the water can follow a large number of reorganization pathways. Thus, the use of enantiomers has a profound effect on the overall errors associated with the free energy of binding. Small errors for the overall binding energies are obtained since the large error associated with the perturbation in solution is removed.[32] The standard deviation for all solvation simulations over 40 ps, in Table II, is 0.139 kcal, and the standard deviation for all the calculations in the enzyme active site, as reported in Table IV, is 0.081 kcal. Thus, the overall uncertainty in the calculation has been reduced by about 63%.

The agreement between theory and experiment indicates that the parameters developed for the heme–sulfur complex are quite good and may allow for the prediction of the binding of other compounds to CYP101. Furthermore, this agreement indicates that the overall binding of the two enantiomers is reasonably

(28) Pearlman, D. A.; Kollman, P. A. *J. Chem. Phys.* **1990**, *94*, 4532–4545.
(29) Edwards, W. D.; Weiner, B.; Zerner, M. C. *J. Am. Chem. Soc.* **1986**, *108*, 2196–2204.
(30) Sugiyama, K.; Trager, W. F. *Biochemistry* **1986**, *25*, 7336–7343.
(31) Lipscomb, J. D. *Biochemistry* **1980**, *19*, 3590–3599.
(32) Mitchell, M. J.; McCammon, J. *J. Comput. Chem.* **1991**, *12*, 271–275.

represented by the model and can be used to describe the orientations of the enzyme–substrate complex during binding. Representative orientations, from dynamics simulations for each enantiomer, are shown in Figure 2, and the general features of binding can be described as follows. The pyridine ring of each enantiomer forms a hydrogen bond to the hydroxyl group of Tyr96. The pyrrolidine ring can adapt a series of conformations by rotating around the pyridine–pyrrolidine bond (shown by the arrow in Figure 2). The rotamer that is shown for (*R*)-nicotine in Figure 2 is consistent with the optical spectra of nicotine binding. The spectral properties of the nicotine–enzyme complex indicate an increase in low spin porphyrin complex upon binding. These experimental results are presumably due to coordination of the pyridine or pyrrolidine nitrogen with the heme–iron. In Figure 2 the nitrogen of the pyrrolidine ring is in close contact with the iron of the porphyrin and could account for the increase in the low-spin porphyrin complex. This structure is also extremely close to the binding orientation of metyrapone determined by Poulos and Howard[32] using crystallography. Rotation about the pyrrolidine–pyridine bond is hindered by interaction with the I-helix. A portion of the I-helix is shown in Figure 2. Visual analysis indicates that, upon rotation, (*S*)-nicotine has slightly more interaction of the *N*-methyl group with the I-helix (Figure 2b). The (*R*)-enantiomer also interacts with the I-helix, but it approaches closer to the porphyrin, reducing the I-helix–substrate interaction, while still maintaining a hydrogen bond to Tyr96.

While the results described in the last paragraph elucidate the factors important in binding to CYP101, it remains to be determined how oxygen binding may influence regioselectivity. In an attempt to predict qualitatively the regioselectivity of CYP101, we ran constant temperature dynamics at 303 K on each enantiomer with oxygen bound to the iron and monitored the distance between the nicotine hydrogen atoms and the heme bound oxygen atom. Once the simulation is started, each enantiomer rapidly reorients to bind to Tyr-96 through a hydrogen bound to the pyridine nitrogen. This binding brings the pyrrolidine ring in close contact with the lipophilic I-helix above the porphyrin which hinders the rotation of the five-membered ring in the active site. The interaction with the I-helix is exacerbated relative to that observed for the enzyme with no oxygen bound. Thus, for each enantiomer a bimodal distribution of orientations was observed. The orientation in which the cis 5′ proton (Figure 1) is closer than the trans 5′ proton to the porphyrin–iron–oxygen species is termed the cis orientation (This orientation is shown for the (*S*)-enantiomer in Figure 3a.) Likewise when the 5′ proton trans to the pyridine ring is pointed toward the iron–oxygen species it is called the trans orientation (Figure 3b). From each of these orientations the iron–oxygen species can abstract a hydrogen from the *N*-methyl group although the mean distance is greater than for the 5′-methylene hydrogens. The mean distance from the heme oxygen for each hydrogen atom is shown in Table V. The mean distances for each position on the (*R*)- and the (*S*)-nicotine predict that the regioselectivity will be 5′ > methyl group oxidation. The experimental regioselectivity for (*R*)- and (*S*)-nicotine agree with this prediction (see Table IV). The sampling of possible orientations appears to be too small for the (*S*)-enantiomer at 303 K. This results in the (*S*)-enantiomer remaining in the trans binding orientation for the majority of the simulation.

In the experimental studies, the hydrogen atom at the 2′-carbon is not abstracted to any measurable extent from the either nicotine enantiomer; however, the mean distance is 4.29 Å for (*R*)-nicotine and 4.67 Å for (*S*)-nicotine. These mean values are close to those for the positions that do react. Thus, this position would be expected to be subjected to oxidation. However, this contradiction is resolved by further analysis of the data that shows that the hydrogen bond between the Tyr96 and the pyridine ring keeps the 2′ proton from approaching closer than 2.6 Å for the (*S*)-enantiomer and 2.0 Å for the (*R*)-enantiomer at any time during the simulation, while all positions that are normally metabolized approach within 2 Å or less (see Table VI).

Collins et al. used the number of times a hydrogen atom approached a certain distance to the iron–oxygen species to predict

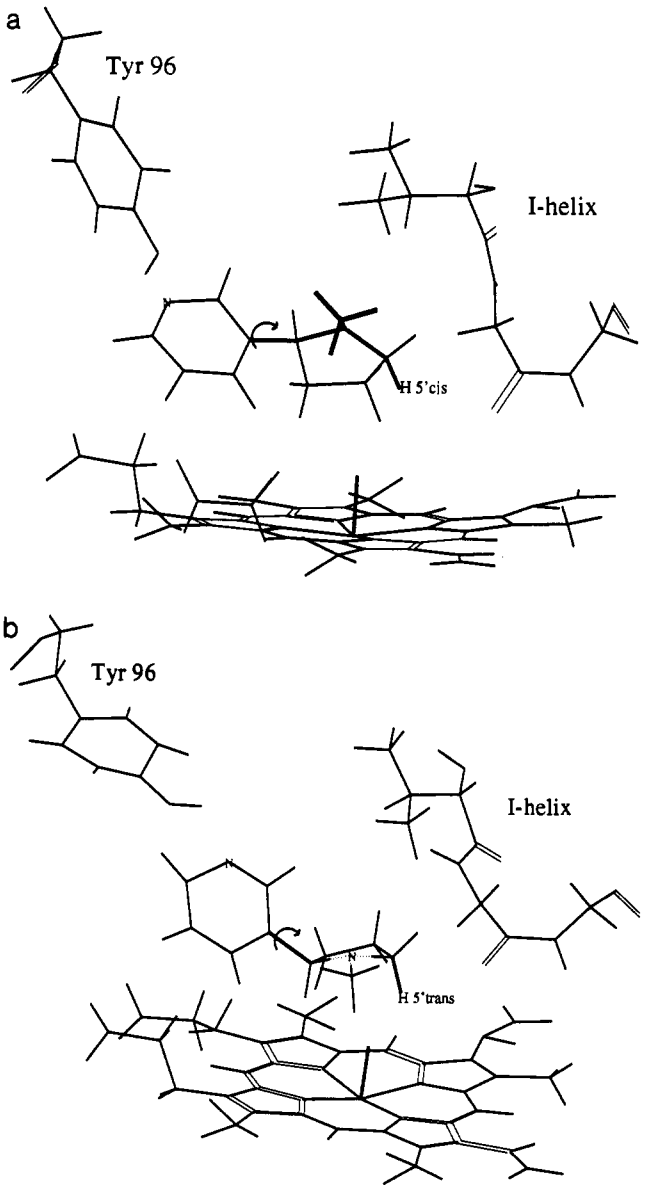

Figure 3. (a) The (*S*)-enantiomer binding in the cis orientation to CYP101 with the oxygen bound. The nitrogen of the pyrrole ring is not labeled to increase the clarity of the illustration. (b) The (*R*)-enantiomer binding to CYP101 with oxygen bound.

the reactivity of valproic acid with CYP101.[10] If we take a similar approach we can attempt to predict the relative reactivity of each enantiomer at a given position of the nicotine enantiomers. In an attempt to increase the number of binding modes that could be recorded in a given simulation time, we increased the temperature of the simulations to 1000 K. At this temperature each of the two distinct binding modes was found to convert to the other binding mode numerous times over a 40-ps simulation. Furthermore, another mode that includes an orientation in which the methyl group can approach the active oxygen species is observed. The results are given in Table VI. The following general conclusions that can be drawn from Table VI that agree with experiment are as follows: the 5′ trans abstraction product of the (*R*)-enantiomer should be favored over the (*S*)-enantiomer, the 5′ cis abstraction product from the (*R*)-enantiomer should be favored over this product for the (*S*)-enantiomer, and the order of regioselectivity for the (*R*)-enantiomer is predicted to be 5′ trans > *N*-methyl > 5′ cis. The overall product ratios will have of course been weighted by the fact that the (*R*)-enantiomer binds with a higher affinity than the (*S*)-enantiomer. All these theoretical results are consistent with the experimental observations. Preliminary results[34] indicate, that at least for the (*S*)-enantiomer, the 5′ trans proton is abstracted at a higher rate than the 5′ cis

proton by CYP101. This is also consistent with results from metabolic studies with mammalian CYP enzymes.[35] Furthermore, the slow rotation between the 5′ cis and 5′ trans binding orientations that are observed at lower temperatures are consistent with the small intramolecular deuterium isotope effects observed at the 5′ position.[35] The following results do not agree with experiment. The ratio of the methyl group oxidation for the (*S*)-enantiomer is predicted to be higher than that at the 5′ positions, and the methyl group of the (*S*)-enantiomer is predicted to be more reactive than the methyl group of the (*R*)-enantiomer. However, the mean values determined at 303 and 1000 K do predict the correct rank order of methyl group to 5′ oxidation. The overprediction of methyl group oxidation for the 1000 K simulation is most likely a result of the increased population of the high-energy binding mode with the methyl group approaching the oxygen (vide supra). These results might be improved if a longer simulation at a lower temperature was performed.

Conclusions

Both binding affinity and regioselectivity are predicted by the dynamics methods reported here although some discrepancies are observed. It is interesting to note that the theoretical calculations were performed prior to obtaining the experimental results and the majority of the theoretical discussion on regioselectivity was written without any knowledge of the experimental results on regioselectivity. Thus, we were able to predict the relative binding affinities, specific steric interactions, and the regioselectivity of the two enantiomers of nicotine. When these methods are combined with the quantum chemical techniques of Korzekwa et al.,[6] a complete picture of the factors that govern small molecule reactivity with the iron–oxygen species of CYP begins to emerge.

Acknowledgment. This work was aided in part by Grant No. IRG-18 from the American Cancer Society (J.P.J.), a pilot Grant ES0124716B (J.P.J.), a grant from the Pittsburgh Supercomputing Center through the NIH Division of Research Resources cooperative agreement 1 P41 RR06009-01 and through a grant from the National Science Foundation Cooperative agreement ASC-8500650 (J.P.J.), and NIH Grant GM-36922 (W.F.T.). We would also like to thank Dr. B. M. Goldstein for helpful comments on this manuscript. The authors can be contacted at jpj@lotus.medicine.rochester.edu.

Supplementary Material Available: The input files required to reproduce the heme and nicotine parameters (Prep files for AMBER) (4 pages). Ordering information is given on any current masthead page.

(33) Poulos, T. L.; Howard, A. J. *Biochemistry* **1987**, *26*, 8165-8174.
(34) Carlson, T. Dissertation, University of Washington, 1992.
(35) Peterson, L. A.; Trevor, A.; Castignoli, N. *J. Med. Chem.* **1987**, *30*, 249-254.

Mechanism of Proton Abstraction in Biotin-Dependent Carboxylation Reactions†

Donald J. Kuo and Irwin A. Rose*

Contribution from the Institute for Cancer Research, Fox Chase Cancer Center, Philadelphia, Pennsylvania 19111. *Received August 3, 1992*

Abstract: Transcarboxylase (E-biotin) in T water is diluted into methylmalonyl CoA (MMCoA) in normal water to determine by isotope capture whether enzyme or solvent provides the proton required to form the product, propionyl CoA. This half-reaction

$$\text{E-biotin·methylmalonyl CoA} \overset{H^+}{\rightleftharpoons} \text{E-biotin-}CO_2^-\text{·propionyl CoA}$$

is followed, in the presence of pyruvate, by formation of oxalacetic acid and free propionyl CoA with regeneration of E-biotin, the three events required for another cycle of reaction with MMCoA. In the absence of pyruvate, the half-reaction is completed by dissociation of propionyl CoA and the reaction is limited to one cycle by the stability of the E-biotin-CO_2. The pulse–chase experiment with T enzyme shows that close to 1 enzyme equiv of T is derived from the pulse and used in the formation of propionyl CoA in the absence of pyruvate. Therefore, an enzyme donor site is protonated in the absence of substrate for transfer after carboxyl transfer to a presumed stabilized carbanionic precursor of the product. The group appears to be *monoprotonic* for two reasons: (1) No additional T is captured with added pyruvate, which greatly increases the rate of release of the propionyl CoA and should allow the donor site to be sampled for T by subsequent cycles of reaction with MMCoA. This is especially to be expected given the slow dissociation (or exchange) rate of the first T, i.e. $k_{ex} \cong 0.2k_{cat}$ at 0 °C. (2) No additional T is captured in the absence of pyruvate when malonyl CoA instead of MMCoA is used in the chase solution. The three methyl protons of acetyl CoA should have provided an expanded pool with which T of a polyprotonic donor would have equilibrated in the one turnover. Other enzyme protons within hydrogen bond distance to the donor site must exchange rapidly before the second turnover. The earlier observation of a small amount of T transfer from 3T pyruvate to propionyl CoA in a complete reaction mixture (Rose, I. A.; O'Connell, E. L.; Solomon, F. *J. Biol. Chem.* **1976**, *251*, 902-904) probably results from enolization of the pyruvate occurring on the oxalacetate subunit in the E·MMCoA·pyruvate complex. The transfer of T would occur if, before the propionyl CoA departs, the donor site is regenerated within the ternary complex from a common pool of protons with which the abstracted T can exchange. These protons would be lost during product liberation, since only one T can be captured from ET in the presence of pyruvate.

Introduction

The mechanism of proton abstraction from substrates to make them acceptors for carboxylation in carboxybiotin-dependent reactions is not well understood. A carbanion intermediate mechanism is indicated for transcarboxylase (methylmalonyl CoA:pyruvate carboxytransferase, E.C. 2.1.3.1), which catalyzes conversion of added enolpyruvate to pyruvate if MMCoA is also present[1] and which produces HF and acrylyl CoA when one attempts to carboxylate β-fluoropropionyl CoA.[2] Proton activation, as shown by α-proton exchange, does not occur unless biotin-dependent enzymes are used in the carboxybiotin form.[1,3]

* Address correspondence to Dr. Irwin A. Rose, Institute for Cancer Research, Fox Chase Cancer Center, 7701 Burholme Avenue, Philadelphia, PA 19111. Telephone: 215-728-2190. FAX: 215-728-3655.
† Dedication: We dedicate this to Harland G. Wood (1907-1991) in appreciation of his many elegant contributions to our understanding of the action of CO_2 in metabolism and especially for his contributions to structural and mechanistic studies of transcarboxylase.

(1) Kuo, D. J.; Rose, I. A. *J. Am. Chem. Soc.* **1982**, *104*, 3235-3236.
(2) Stubbe, J.; Fish, S.; Abeles, R. H. *J. Biol. Chem.* **1980**, *255*, 236-242.

0002-7863/93/1515-387$04.00/0